GEOLOGY | THE GEOLOGICAL SOCIETY OF AMERICA®

https://doi.org/10.1130/G48696.1

Manuscript received 27 June 2020
Revised manuscript received 7 December 2020
Manuscript accepted 14 January 2021

Published online 22 March 2021

Maturation experiments reveal bias in the chemistry of fossil melanosomes

Valentina Rossi[1*†], Samuel M. Webb[2] and Maria McNamara[1*]
[1]School of Biological, Earth and Environmental Sciences, University College Cork, Cork T23 TK30, Ireland
[2]Stanford Synchrotron Radiation Lightsource (SSRL), SLAC National Accelerator Laboratory, Menlo Park, California 94025, USA

ABSTRACT

Fossil melanosomes are a major focus of paleobiological research because they can inform on the original coloration, phylogenetic affinities, and internal anatomy of ancient animals. Recent studies of vertebrate melanosomes revealed tissue-specific trends in melanosome-metal associations that can persist in fossils. In some fossil vertebrates, however, melanosomes from all body regions are enriched only in Cu, suggesting diagenetic overprinting of original chemistry. We tested this hypothesis using laboratory experiments on melanosomes from skin and liver of the African clawed frog *Xenopus laevis*. After maturation in Cu-rich media, the metal chemistry of melanosomes from these tissues converged toward a common composition, and original differences in Cu oxidation state were lost. Elevated Cu concentrations and a pervasive Cu(II) signal are likely indicators of diagenetically altered melanosomes. These results provide a robust experimental basis for interpretating the chemistry of fossil melanosomes.

INTRODUCTION

Fossil color is a major focus of paleobiological research (Roy et al., 2019). Melanosomes, micron-sized organelles rich in melanin *in vivo*, are preserved in diverse fossil taxa and tissues (Vinther et al., 2008; Lindgren et al., 2012; Manning et al., 2019; Rogers et al., 2019; Rossi et al., 2019) and provide information about the evolution of color (Li et al., 2014; Gabbott et al., 2016; Lindgren et al., 2018; Manning et al., 2019) and the internal anatomy (Rossi et al., 2019) and phylogenetic affinities (Clements et al., 2016; Rogers et al., 2019) of ancient animals.

Melanosomes typically show tissue-specific metal associations in extant (Edwards et al., 2016; Rossi et al., 2019) and some fossil vertebrates (Wogelius et al., 2011; Manning et al., 2019; Rossi et al., 2019). Other fossil vertebrates, however, show widespread Cu enrichment in melanosomes from all tissues (Rossi et al., 2020). This renders anatomical interpretation difficult and questions whether melanosome-associated Cu in other fossils is original or reflects, at least in part, diagenetic binding of Cu to degraded melanin. Some fossil melanosomes are rich in metals absent from the melanosomal metal inventory in extant vertebrates (Rogers et al., 2019; Rossi et al., 2019). Collectively, these data suggest that the preserved metal complement of melanosomes in some vertebrate fossils has been altered by diagenetic overprinting. This has not been tested, precluding interpretation of preserved chemical signatures in fossil melanosomes.

We used taphonomic experiments on amphibian melanosomes to test whether the melanosomal metal inventory alters during maturation. Our results reveal significant alteration of original melanosome chemistry and identified the features that are likely to be taphonomic.

METHODS

Study Design

We analyzed the chemistry of melanosomes from the skin and liver of the extant frog *Xenopus laevis*. Melanosomes from these tissues differ chemically. Skin melanosomes are enriched in Ca and Zn; liver melanosomes are enriched in Fe and Cu (Rossi et al., 2019). Experiments (Ito et al., 2013) on *Sepia* (cuttlefish) melanin reveal that maturation alters eumelanin and its associated metal inventory; experiments on vertebrate eye melanosomes reveal diagenetic alteration of Cu:Zn ratios (Rogers et al., 2020). No comparable studies exist for other vertebrate tissues. Our experiments were aimed to investigate the comparative impact of maturation on the metal content of melanosomes from different vertebrate tissues. Decay was not considered because it does not impact melanosome geometry (McNamara et al., 2018), and impacts on melanosome chemistry are likely to be minimal relative to that of maturation. Pressure and temperature were not varied in our experiments because the impact of these parameters on melanosomes during maturation has been investigated previously (McNamara et al., 2013; Colleary et al., 2015). Our experiments focused on Cu, which can dominate the metal inventory of fossils (Rossi et al., 2020). As in previous studies on *Sepia* melanin, the Cu solution we used was concentrated relative to natural pore fluids (Wong, 1983) to ensure availability of sufficient Cu during the experiment (Liu and Simon, 2005; Hong and Simon, 2007). The experimental conditions used were almost identical to those of Slater et al. (2020) (differing only in pressure: 130 bar [this study] versus 135 bar [Slater et al., 2020]), and they were selected to ensure retention of intact melanosomes after the experiment, not to simulate conditions associated with specific fossil localities.

Maturation Experiments

Melanosome extracts (see the Supplemental Material[1]) from the skin and liver of the extant frog *Xenopus laevis* were placed in gold capsules ($n = 12$) with 8–12 μL of distilled deionized (DD) water (pH = 7.8) or a 16 m*M* solution of Cu in HNO_3 (Sigma-Aldrich analytical

*E-mails: valentina.rossi@naturmuseum.it; maria.mcnamara@ucc.ie

†Current address: Naturmuseum Südtirol, via Bottai 1, I-39030, Bolzano, Italy

[1]Supplemental Material. Supplemental text and discussion, figures of scanning electron microscope photos of untreated and matured melanosomes, analysis of thickness, multichannel analysis of X-ray fluorescence, and datasets with melanosome geometry and chemistry. Please visit https://doi.org/10.1130/GEOL.S.14143991 to access the supplemental material, and contact editing@geosociety.org with any questions.

CITATION: Rossi, V., Webb, S.M., and McNamara, M., 2021, Maturation experiments reveal bias in the chemistry of fossil melanosomes: Geology, v. 49, p. 784–788, https://doi.org/10.1130/G48696.1

standard; here termed "Cu-solution"; pH = 3). Capsules were welded shut and matured at 200 °C, 130 bar (13 MPa) for 24 h in a StrataTech custom-built high-pressure rig. Matured extracts were air-dried for 8 h.

Scanning Electron Microscopy (SEM)

Micrographs were obtained using a JEOL IT100 VP-SEM at an accelerating voltage of 10 kV and working distance of 10 mm. Long- and short-axis measurements were taken for 50 melanosomes per sample, orientated perpendicular to line of sight and in focus.

Micro-Synchrotron Rapid Scanning–X-Ray Fluorescence Analysis (Micro-SRS-XRF)

Melanosome extracts were placed on low-sulfur tape and analyzed at the Stanford Synchrotron Radiation Lightsource (SSRL) using synchrotron rapid scanning–X-ray fluorescence analysis at beam line 2–3 (see the Supplemental Material). The fluorescence spectrum was collected for each data point, and the intensity of fluorescence lines for selected elements (P, Ca, Ti, Mn, Fe, Ni, Cu, and Zn) was monitored using a silicon drift Vortex detector. Data were processed using MicroAnalysis Toolkit software (SMAK 1.50, Webb, 2011). Spectra were analyzed using the Multi-Channel Analysis (MCA) spectral fitting function in the MicroAnalysis Toolkit, which uses the PyMCA algorithm (Solé et al., 2007). Regions of interest (ROIs) for quantitative analysis were selected from each sample. Elemental concentrations were calibrated using U.S. National Institute of Standards and Technology (NIST)–traceable thin film standards (MicroMatter, Vancouver, Canada). For each ROI, metal concentrations per pixel were calculated using standard protocols (i.e., calculated via a linear regression of the area of the MCA trace), and median and interquartile range (IQR) values were calculated for each element.

Statistical Analysis

One replicate of liver melanosomes matured in DD water exhibited anomalously high concentrations for all elements and was omitted from the statistical analysis. Concentration data for the remaining samples were log-transformed to meet assumptions of normality required by linear discriminant analysis (LDA) and Welch's analysis of variance (ANOVA). Models were validated using residual plots in R (R Core Team, 2013). Chemical differences among samples were visualized using LDA and Welch's ANOVA. Differences in the geometry of melanosomes among all extracts were tested using ANOVA and *t*-tests in R.

X-Ray Absorption Near Edge Structure Spectroscopy (XANES)

Three points in the XRF map for Cu from each extract were analyzed further. Selected points were representative of the mean concentration for that sample. Three consecutive XANES spectra were collected at each point at beamline 2–3 at SSRL by driving the incident beam energy through the Cu K edge in a stepwise fashion using a step size of 10 eV from 8749 to 8958 eV (pre-edge), 0.35 eV from 8959 to 9006 eV (across the Cu K edge), and 10 eV from 9007 to 9020 eV (postedge) and recording

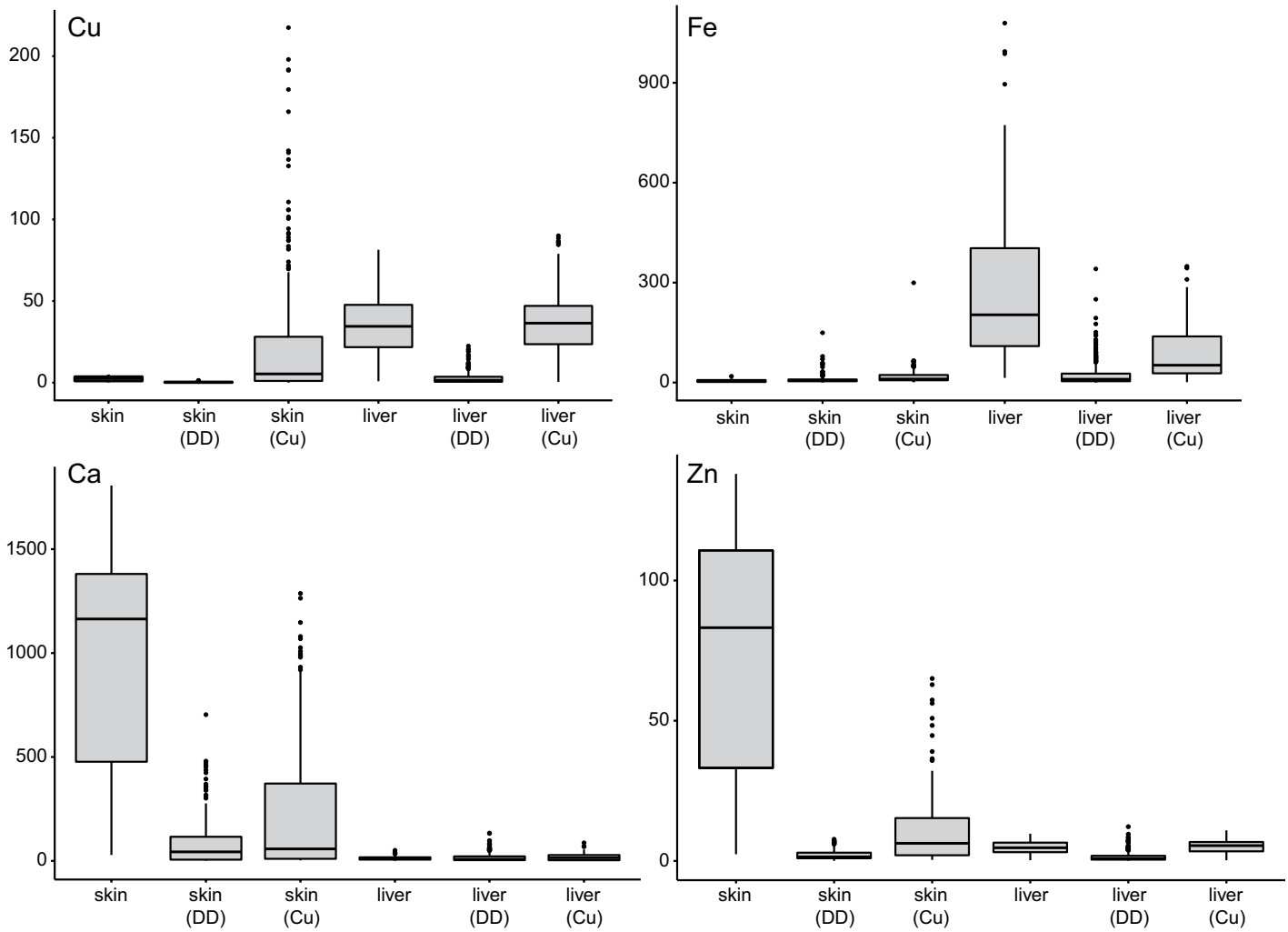

Figure 1. Box plots of micro-synchrotron rapid scanning–X-ray fluorescence analysis (micro-SRS-XRF) data for untreated and matured melanosomes from the frog *Xenopus laevis* skin and liver. DD—distilled deionized water; Cu—Cu-solution.

the emitted intensity of the Kα line as a function of incident energy. The three spectra for each sample showed no change in peak position or signal intensity that would evidence beam damage. The monochromator energy was calibrated using a Cu foil. Spectra were processed using Athena software (Ravel and Newville, 2005).

RESULTS

XRF spectra showed well-constrained K emission peaks for Ca, Fe, Zn, and Cu. Peaks for P and Ti were absent, and those for Mn and Ni occurred in only two spectra (see Supplemental Material); these four elements were thus not considered further.

Concentrations of Ca, Fe, Cu, and Zn varied among extracts (Fig. 1; see the Supplemental Material). These elements are frequently associated with melanosomes in extant vertebrates (Rossi et al., 2019). Untreated melanosomes from different tissues were separated in chemospace (Fig. 2): untreated skin melanosomes were enriched in Ca (median = 1160 μg/cm² [skin]; 11 μg/cm² [liver]) and Zn (83 μg/cm² [skin]; 4.6 μg/cm² [liver]). Liver melanosomes were enriched in Fe (203 μg/cm² [liver], 5.4 μg/cm² [skin]) and Cu (34 μg/cm² [liver], 2.5 μg/cm² [skin]) (Fig. 1). The data for extracts matured in DD water converged and overlapped close to the center of the chemospace: Skin melanosomes were depleted in Ca (43.5 μg/cm²) and Zn (1.4 μg/cm²), and liver melanosomes were depleted in Fe (9.8 μg/cm²) and Cu (0.2 μg/cm²) (Fig. 1). Melanosomes matured in Cu solution also converged in chemistry, due primarily to an increase in Cu concentrations in matured melanosomes (skin: 5 μg/cm²; liver: 36 μg/cm²) and, specifically for skin melanosomes, substantial loss of Ca (57.7 μg/cm²) and Zn (6.2 μg/cm²) relative to untreated samples (Fig. 1). Somewhat surprisingly, liver melanosomes matured in Cu solution showed a considerable loss of Fe (from 203 μg/cm² to 52 μg/cm²) but no significant increase in Cu compared to untreated melanosomes (from 34 μg/cm² to 36 μg/cm², respectively). Differences between untreated and matured samples from each tissue were statistically significant in most cases (Table 1).

XANES spectroscopy revealed variation in Cu oxidation state among untreated and matured melanosomes, and among melanosomes from different tissues (Fig. 3). Untreated skin melanosomes showed a broad region of absorbance from ~8980 to 9000 eV; the region of maximum absorbance at ~8994.0–8995.8 eV indicates a dominant contribution from Cu(II), but the prominent shoulder at ~8980 eV indicates a contribution from Cu(I). Maturation in DD water did not alter this absorbance profile, but maturation in Cu solution resulted in loss of the shoulder at ~8980 eV, yielding a spectrum with a single peak centered at 8994 ± 1 eV, indicating strong contributions from Cu(II) only. The spectrum for untreated liver melanosomes exhibited broad absorbance at ~8980–9000 eV but lacked the shoulder at ~8980 eV and the peak at ~8994 eV, suggesting contributions from Cu(I) and Cu(II) but potentially in a different ratio, or with a different binding environment, compared to Cu in the skin melanosomes. Maturation in Cu solution did not alter the profile of the liver XANES spectrum; maturation in DD water generated a minor pre-edge peak at ~8980 eV, indicating an enhanced contribution from Cu(I) (Fig. 3).

DISCUSSION

Our results confirm that the metal inventory (i.e., metallome) of melanosomes can be altered during maturation and that melanosomes from two *Xenopus* tissues respond differently to changes in ambient chemistry. Tissue-specific melanosome chemistries can alter during diagenesis via the loss of intrinsic metals associated with melanin in vivo and the incorporation of extrinsic metals. Following maturation, Ca and Zn are depleted in skin melanosomes; Fe (and, for experiments in DD water, Cu) were depleted in liver melanosomes. This almost certainly reflects changes in the chemical stability of the metallome of melanin upon heating, where changes in ambient pH and metal availability can induce loss of melanin-bound metals (e.g., via maturation in DD water; Hong and Simon, 2007). It is not possible, however, to separate the respective contributions of heating and pH to the loss of melanin-associated elements due to the nature of our experimental setup.

Alteration of the melanin metallome is linked to the metal binding affinity of specific

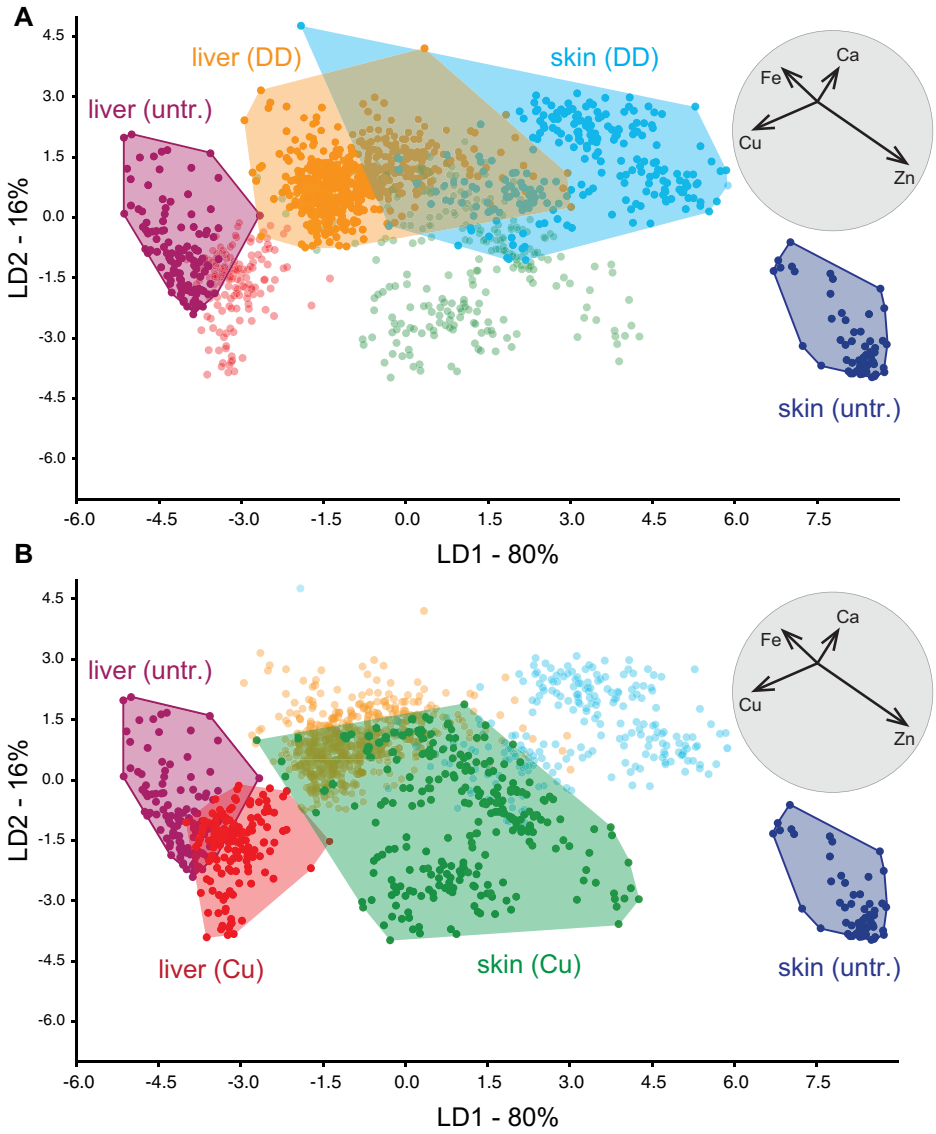

Figure 2. Linear discriminant analysis (LDA) of micro-synchrotron rapid scanning–X-ray fluorescence analysis (micro-SRS-XRF) data for melanosomes from the frog *Xenopus laevis* skin and liver. Data are highlighted for untreated melanosomes (untr.; A, B) and melanosomes matured in distilled deionized (DD) water (A) and in Cu solution (Cu; B). Gray circle is biplot showing contribution of each element (vectors) to separation of groups. Wilk's lambda test = 0.03.

TABLE 1. WELCH'S ANOVA AND POST-HOC TEST OF VARIATION IN SYNCHROTRON RAPID SCANNING–X-RAY FLUORESCENCE ANALYSIS (SRS-XRF) CONCENTRATIONS OF KEY ELEMENTS

Welch's analysis of variance (ANOVA)	Ca	Cu	Fe	Zn
p-value	**1.53 E–93**	**9.9 E–213**	**2.4 E–126**	**1.80 E–116**
denom df	341.22	347	340.3	338.68
num df	5	5	5	5
Games-Howell post-hoc test pair	**Cu**	**Fe**	**Ca**	**Zn**
Skin (Cu)–liver (Cu)	**1.00E–15**	**5.77E–13**	**1.00E–15**	0.39
Liver (DD)–liver (Cu)	**7.05E–11**	**9.10E–13**	0.545	**1.00E–15**
Skin (DD)–liver (Cu)	**1.00E–15**	**9.26E–13**	**1.00E–15**	**1.00E–15**
Liver–liver (Cu)	0.607	**3.30E–13**	1	0.397
Skin–liver (Cu)	**1.00E–15**	**4.13E–10**	**4.83E–10**	**1.00E–15**
Liver (DD)–skin (Cu)	**1.00E–15**	0.098	**1.00E–15**	**1.00E–15**
Skin (DD)–skin (Cu)	**1.00E–15**	**7.08E–11**	**0.000174**	**1.00E–15**
Liver–skin (Cu)	**1.00E–15**	**1.98E–14**	**1.00E–15**	**0.014**
Skin–skin (Cu)	**3.59E–09**	**6.96E–10**	**2.53E–14**	**2.25E–10**
Skin (DD)–liver (DD)	**1.00E–15**	**2.23E–07**	**1.02E–13**	**1.56E–10**
Liver–liver (DD)	**2.72E–13**	**2.42E–13**	0.373	**1.00E–15**
Skin–liver (DD)	0.81	**1.98E–07**	**1.00E–15**	**1.63E–11**
Liver–skin (DD)	**1.00E–15**	**1.99E–13**	**1.00E–15**	**4.43E–13**
Skin–skin (DD)	**1.00E–15**	**0.01**	**1.00E–15**	**1.00E–15**
Skin–liver	**3.54E–10**	**3.77E–10**	**1.00E–15**	1.00E–15

Note: Bold text represents statistically significant *p* values. Cu—Cu-solution; DD—distilled deionized water; df—degrees of freedom.

bonds (Hong et al., 2004). For *Sepia* melanin, Ca and Zn usually bind to carboxyl groups, Fe binds to amine groups, and Cu binds to phenol groups. Changes in ambient conditions, however, can alter these associations (Hong and Simon, 2007). In *Sepia*, at pH 3–4 and with abundant aqueous Cu (Hong and Simon, 2007), melanin can bind Cu at amine and carboxyl groups, triggering release of Ca, Zn, and Fe (Hong and Simon, 2007). Our experiments confirm that these patterns in metal-melanin binding apply to *Xenopus* skin melanosomes: Following maturation at pH 3 and with abundant aqueous Cu, concentrations of melanosome-associated Cu increased, but concentrations of all other elements substantially decreased. This is consistent with the hypothesis that Cu has substituted Zn and Ca in the melanin structure (see Hong and Simon, 2007). Matured melanosomes showed no evidence for Cu microprecipitates, suggesting the Cu was organically bound.

Our experiments used concentrated Cu-rich media and were not intended to replicate metal concentrations in fossil melanosomes. Direct comparison of our data with Cu concentration values reported for fossil melanosomes is thus not appropriate. Instead, our experiments illuminate patterns of Cu enrichment in fossils. Enrichment in Cu (but not in other elements) in all melanosome-bearing body regions in some vertebrate fossils (Rossi et al., 2020) can be explained by our experiments, which showed preferential uptake of Cu by skin melanosomes and significant loss of other elements. This resulted in chemical convergence between tissues that originally differed in chemistry. The enrichment in Cu in some fossil vertebrate melanosomes and the loss of tissue-specific signals apparent in modern vertebrates (Rossi et al., 2020) thus likely reflect increased association of Cu with melanosomes (especially from integumentary tissues) during diagenesis. Changes in pH alone could potentially alter the melanosome metallome, but analysis of the pH of the experimental medium during and after the experiment was not possible. Thus, we cannot exclude the possibility that pH changes contributed to our results.

Regardless, these data have critical implications for interpretation of fossil melanosome

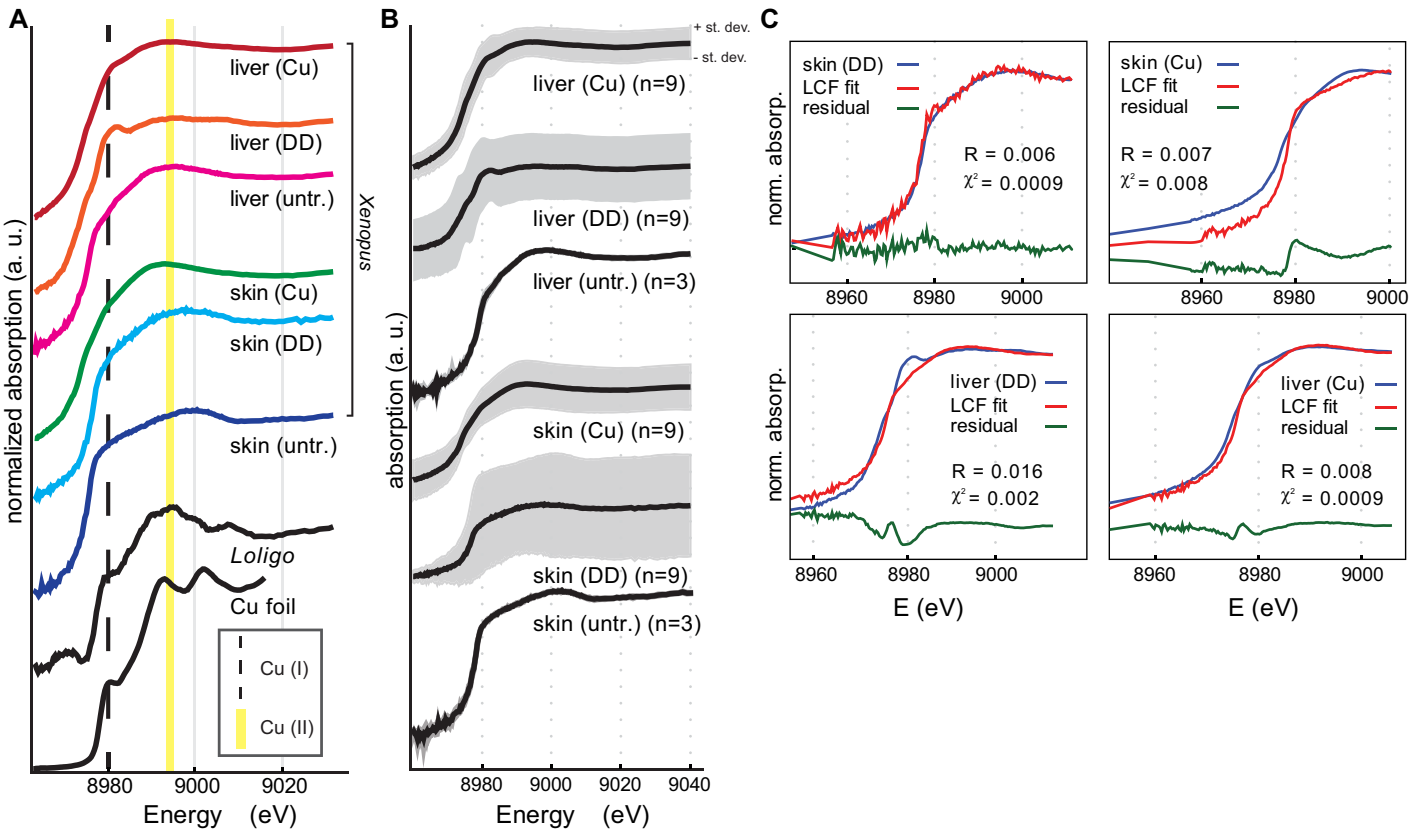

Figure 3. Copper X-ray absorption near edge structure spectroscopy (XANES) analyses of experimental data. (A) Spectra of Cu foil, *Loligo* (squid) melanin (modified from Rogers et al., 2019), and untreated and matured melanosomes from *Xenopus laevis* (frog) skin and liver. (B) Averaged spectra of samples and standard deviation. (C) Linear combination fitting (LCF) of matured samples; residuals were used to identify Cu(I) peaks. DD—distilled deionized water; Cu—Cu solution; untr.—untreated.

chemistry. The diagenetic bias in Cu incorporation and associated loss of tissue-specific chemical signals between skin and liver melanosomes render discrimination of skin and internal melanosomes difficult in fossils that have experienced overprinting of original chemistry by Cu incorporation.

Our Cu-XANES spectra indicate that the Cu associated with the melanosome extracts is consistent with a mixture of Cu(I) and Cu(II). Cu(II) is commonly associated with melanin (Hong and Simon, 2007; Wogelius et al., 2011). Cu(I) can also associate with natural melanins (Rogers et al., 2019); chelation of reduced metals by melanin may relate to protective functions against catalysis of Fenton reactions (Hong and Simon, 2007). The minor contributions from Cu(I) in our untreated extracts may, therefore, be biological and not an analytical artifact.

All extracts were analyzed under identical conditions; differences in the spectral profiles of the melanosomes analyzed are thus likely to be real. Intriguingly, our study showed differences in the response of skin and liver melanosomes to maturation in Cu solution: The spectral profile for matured skin melanosomes changed markedly to a profile consistent with a dominant Cu(II) contribution, whereas that for matured liver melanosomes was unaltered. This supports the hypothesis that Cu is preferentially taken up by skin melanosomes and suggests that the "additional" Cu is primarily Cu(II). Cu-XANES and Cu-EXAFS (extended X-ray absorption fine structure) (Wogelius et al., 2011) may therefore aid in the identification of original versus diagenetic Cu in fossil melanosomes.

In conclusion, our study provides the first experimental evidence that diagenetic processes can alter the metal inventory of melanosomes. An understanding of the chemical taphonomy of melanosomes is therefore critical to interpreting preserved metal signatures in fossils. The combination of enrichment of melanosomes from most/all body regions in Cu and a homogeneous, strong Cu(II) signal in XANES spectra is likely to indicate diagenetic alteration. These results serve as a model to assess the extent of diagenetic overprinting of original melanosome chemistry. This will aid the identification of fossil biotas that may retain components of original melanosome chemistry and thus are targets for studies of fossil color.

ACKNOWLEDGMENTS

We thank N. Edwards and S. Bone for technical assistance, and R. Wogelius, P. Geuriau, and two anonymous reviewers for discussion. This work was funded by European Research Council Starting Grant ERC-2014-StG-637691-ANICOLEVO awarded to McNamara. Use of the Stanford Synchrotron Radiation Lightsource, SLAC National Accelerator Laboratory, is supported by the U.S. Department of Energy, Office of Science, Office of Basic Energy Sciences under contract DE-AC02–76SF00515, under proposal 5072 awarded to McNamara.

REFERENCES CITED

Clements, T., Dolocan, A., Martin, P., Purnell, M.A., Vinther, J., and Gabbott, S.E., 2016, The eyes of *Tullimonstrum* reveal a vertebrate affinity: Nature, v. 532, p. 500–503, https://doi.org/10.1038/nature17647.

Colleary, C., et al., 2015, Chemical, experimental, and morphological evidence for diagenetically altered melanin in exceptionally preserved fossils: Proceedings of the National Academy of Sciences of the United States of America, v. 112, p. 12592–12597.

Edwards, N.P., Van Veelen, A., Anné, J., Manning, P.L., Bergmann, U., Sellers, W.I., Egerton, V.M., Sokaras, D., Alonso-Mori, R., and Wakamatsu, K., 2016, Elemental characterisation of melanin in feathers via synchrotron X-ray imaging and absorption spectroscopy: Scientific Reports, v. 6, p. 34002, https://doi.org/10.1038/srep34002.

Gabbott, S.E., Donoghue, P.C., Sansom, R.S., Vinther, J., Dolocan, A., and Purnell, M.A., 2016, Pigmented anatomy in Carboniferous cyclostomes and the evolution of the vertebrate eye: Proceedings of the Royal Society B–Biological Sciences, v. 283, p. 20161151, https://doi.org/10.1098/rspb.2016.1151.

Hong, L., and Simon, J.D., 2007, Current understanding of the binding sites, capacity, affinity, and biological significance of metals in melanin: The Journal of Physical Chemistry B, v. 111, p. 7938–7947, https://doi.org/10.1021/jp071439h.

Hong, L., Liu, Y., and Simon, J.D., 2004, Binding of metal ions to melanin and their effects on the aerobic reactivity: Photochemistry and Photobiology, v. 80, p. 477–481, https://doi.org/10.1562/0031-8655(2004)080<0477:BOMITM>2.0.CO;2.

Ito, S., Wakamatsu, K., Glass, K., and Simon, J.D., 2013, High-performance liquid chromatography estimation of cross-linking of dihydroxyindole moiety in eumelanin: Analytical Biochemistry, v. 434, p. 221–225, https://doi.org/10.1016/j.ab.2012.12.005.

Li, Q., Clarke, J.A., Gao, K.-Q., Zhou, C.-F., Meng, Q., Li, D., D'Alba, L., and Shawkey, M.D., 2014, Melanosome evolution indicates a key physiological shift within feathered dinosaurs: Nature, v. 507, p. 350–353, https://doi.org/10.1038/nature12973.

Lindgren, J., Uvdal, P., Sjövall, P., Nilsson, D.E., Engdahl, A., Schultz, B.P., and Thiel, V., 2012, Molecular preservation of the pigment melanin in fossil melanosomes: Nature Communications, v. 3, p. 824, https://doi.org/10.1038/ncomms1819.

Lindgren, J., Sjövall, P., Thiel, V., Zheng, W., Ito, S., Wakamatsu, K., Hauff, R., Kear, B.P., Engdahl, A., and Alwmark, C., 2018, Soft-tissue evidence for homeothermy and crypsis in a Jurassic ichthyosaur: Nature, v. 564, p. 359–365, https://doi.org/10.1038/s41586-018-0775-x.

Liu, Y., and Simon, J.D., 2005, Metal-ion interactions and the structural organization of *Sepia* eumelanin: Pigment Cell Research, v. 18, p. 42–48, https://doi.org/10.1111/j.1600-0749.2004.00197.x.

Manning, P.L., Edwards, N.P., Bergmann, U., Anné, J., Sellers, W.I., van Veelen, A., Sokaras, D., Egerton, V.M., Alonso-Mori, R., and Ignatyev, K., 2019, Pheomelanin pigment remnants mapped in fossils of an extinct mammal: Nature Communications, v. 10, p. 2250, https://doi.org/10.1038/s41467-019-10087-2.

McNamara, M.E., Briggs, D.E.G., Orr, P.J., Field, D.J., and Wang, Z., 2013, Experimental maturation of feathers: Implications for reconstructions of fossil feather colour: Biology Letters, v. 9, p. 20130184, https://doi.org/10.1098/rsbl.2013.0184.

McNamara, M.E., Kaye, J.S., Benton, M.J., Orr, P.J., Rossi, V., Ito, S., and Wakamatsu, K., 2018, Non-integumentary melanosomes can bias reconstructions of the colours of fossil vertebrates: Nature Communications, v. 9, p. 1–9, https://doi.org/10.1038/s41467-018-05148-x.

R Core Team, 2013, R: A language and environment for statistical computing: https://www.R-project.org/ (accessed November 2020).

Ravel, B., and Newville, M., 2005, Athena, Artemis, Hephaestus: Data analysis for X-ray absorption spectroscopy using IFEFFIT: Journal of Synchrotron Radiation, v. 12, p. 537–541, https://doi.org/10.1107/S0909049505012719.

Rogers, C.S., Astrop, T.I., Webb, S.M., Ito, S., Wakamatsu, K., and McNamara, M.E., 2019, Synchrotron X-ray absorption spectroscopy of melanosomes in vertebrates and cephalopods: Implications for the affinity of *Tullimonstrum*: Proceedings of the Royal Society B–Biological Sciences, v. 286, p. 20191649, https://doi.org/10.1098/rspb.2019.1649.

Rogers, C.S., Webb, S.M., and McNamara, M.E., 2020, Synchrotron X-ray fluorescence analysis reveals diagenetic alteration of fossil melanosome trace metal chemistry: Palaeontology, https://doi.org/10.1111/pala.12506 (in press).

Rossi, V., McNamara, M.E., Webb, S.M., Ito, S., and Wakamatsu, K., 2019, Tissue-specific geometry and chemistry of modern and fossilized melanosomes reveal internal anatomy of extinct vertebrates: Proceedings of the National Academy of Sciences of the United States of America, v. 116, p. 17880–17889, https://doi.org/10.1073/pnas.1820285116.

Rossi, V., Webb, S.M., and McNamara, M., 2020, Hierarchical biota-level and taxonomic controls on the chemistry of fossil melanosomes revealed using synchrotron X-ray fluorescence: Scientific Reports, v. 10, p. 8970, https://doi.org/10.1038/s41598-020-65868-3.

Roy, A., Pittman, M., Saitta, E.T., Kaye, T.G., and Xu, X., 2019, Recent advances in amniote palaeocolour reconstruction and a framework for future research: Biological Reviews of the Cambridge Philosophical Society, v. 95, p. 22–50, https://doi.org/10.1111/brv.12552.

Slater, T.S., McNamara, M.E., Orr, P.J., Foley, T.B., Ito, S., and Wakamatsu, K., 2020, Taphonomic experiments resolve controls on the preservation of melanosomes and keratinous tissues in feathers: Palaeontology, v. 63, p. 103–115, https://doi.org/10.1111/pala.12445.

Solé, V., Papillon, E., Cotte, M., Walter, P., and Susini, J., 2007, A multiplatform code for the analysis of energy-dispersive X-ray fluorescence spectra: Spectrochimica Acta: Part B, Atomic Spectroscopy, v. 62, p. 63–68.

Vinther, J., Briggs, D.E., Prum, R.O., and Saranathan, V., 2008, The colour of fossil feathers: Biology Letters, v. 4, p. 522–525, https://doi.org/10.1098/rsbl.2008.0302.

Webb, S., 2011, The MicroAnalysis Toolkit: X-ray fluorescence image processing software: AIP Conference Proceedings, v. 1365, p. 196–199.

Wogelius, R., Manning, P., Barden, H., Edwards, N., Webb, S., Sellers, W., Taylor, K., Larson, P., Dodson, P., and You, H., 2011, Trace metals as biomarkers for eumelanin pigment in the fossil record: Science, v. 333, p. 1622–1626, https://doi.org/10.1126/science.1205748.

Wong, C.S., ed., 1983, Trace Metals in Sea Water, Volume 9: New York, Springer Science & Business Media, 919 p., https://doi.org/10.1007/978-1-4757-6864-0.

Printed in USA